DOI: 10.13009/EUCASS2019-892

Dynamics of generation of nanooxides during the burning of aluminum and titanium microparticles

Reshetnikov Igor, Karasev Vladimir**, Bykovskikh Alla***, Glotov Oleg*****
** ICKC RAS, NSU*
ICKC RAS, Institutskaya 3, Novosibirsk, 630090, Russia; sohat@mail.ru
*** ICKC RAS*
ICKC RAS, Institutskaya 3, Novosibirsk, 630090, Russia; karasev@kinetics.nsc.ru
**** NSU*
NSU, Novosibirsk, Russia
***** ICKC RAS*
ICKC RAS, Institutskaya 3, Novosibirsk, 630090, Russia; glotov@kinetics.nsc.ru

Abstract

The burning of the single Al particles (vapor phase combustion mode) and Ti particles (heterogeneous combustion mode) was studied in this paper. The size range of the studied particles was 100-300 micrometers. The main task of this work was to study the specific features and the rate of generation of nano-oxide smoke as a function of the current time during the combustion of a metal microparticle freely moving in the air. The dependence of the frequency of rotation vs the diameter for Al particles is obtained. The model of rotation of Al particles during the combustion is developed.

1. Introduction

Metal powders are widely used as a fuel in solid propellants. Details of metal combustion mechanisms in a dispersed state are valuable for optimizing the performance of rocket propellant. The developed models of metal particles combustion practically do not specify any details of the time history of oxide generation. However, this diagnostic is an informative technique for specifying the combustion mechanism. In fact, the oxide generation rate indicates the intensity of the combustion and its stage.

The main task of this work was to study the specific features and the rate of generation of nano-oxide smoke as a function of the current time during the combustion of a metal microparticle freely moving in the air. The burning of the single Al particles (vapor-phase combustion mode, Fig. 1, 2) and Ti particles (heterogeneous combustion mode) freely falling in the air was studied in this paper. The size range of the studied particles was 100-300 micrometers.

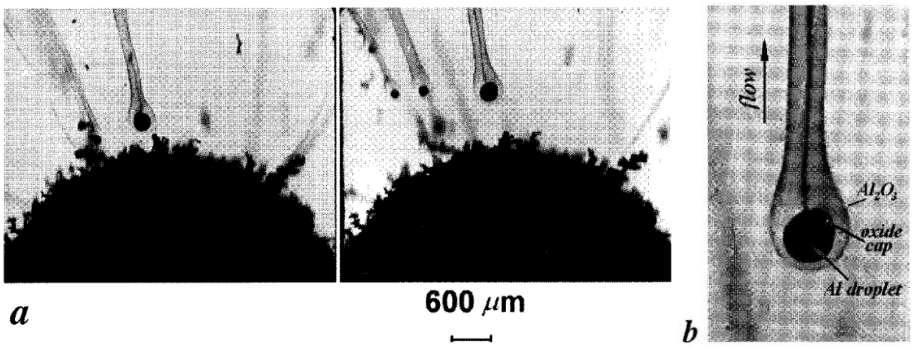

Fig. 1. High-speed photographic data, 2000 frames per second: (a) two consecutive shadow images illustrating generation of agglomerates by the propellant burning surface; (b) magnified showing the Al droplet, oxide cap and Al_2O_3 nanooxide tail.

DOI: 10.13009/EUCASS2019-892

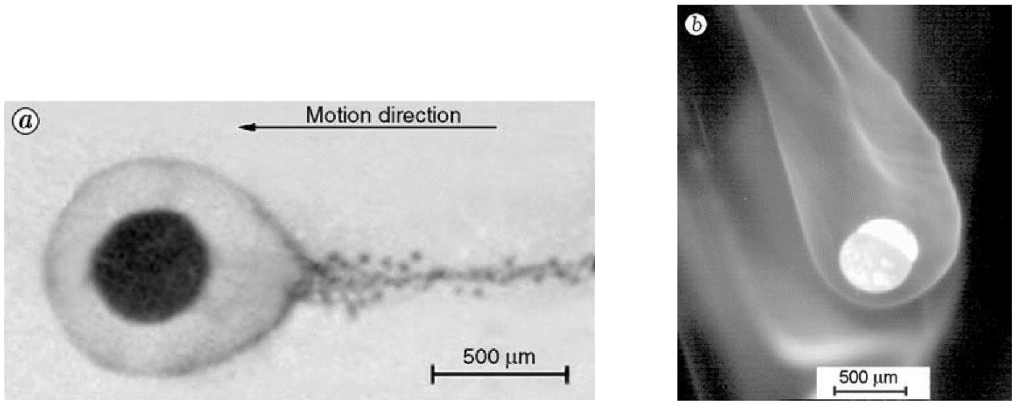

Fig. 2. Burning Al droplet: shadow image behind a blue light filter (a) and in the natural glow (b).

2. Al_2O_3 particle growth

The Al_2O_3 particle growth in the reaction zone is characterized by simultaneous coagulation and coalescence. The resulting nanoparticles are liquid and spherical. In experiments the burning aluminum droplets fall down in the ambient air, creating a tail composed of Al_2O_3 nanoparticles (see Fig. 3). The droplet velocity is about 100 cm/s. This value is too slow to affect considerably the temperature distribution in the reaction zone. At the distance of several radii from the droplet surface the temperature decreases to the Al_2O_3 melting point (Fig. 3).

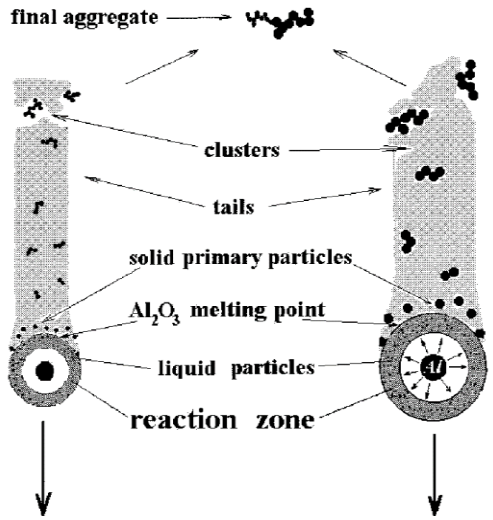

Fig. 3. Scheme of the Al_2O_3 coagulation process.

DOI: 10.13009/EUCASS2019-892

3. TiO_2 and Al_2O_3 aggregates

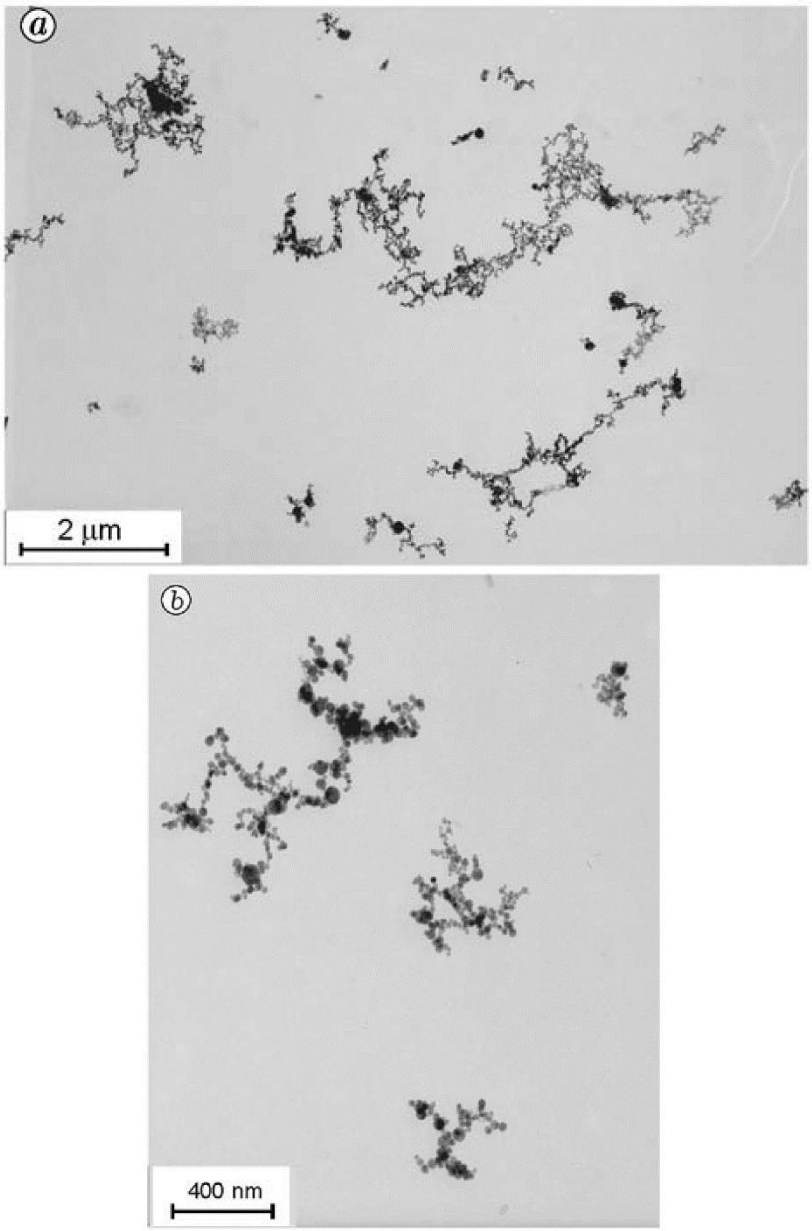

Fig. 4. TiO_2 (a) and Al_2O_3 (b) aggregates sampled from the reaction vessel in 1 min after combustion of the pyrotechnic mixture.

Typical images of the aggregates are given in Fig. 4. X-ray diffraction analysis shows that the crystal structure of the TiO_2 spherules is anatase (60%) and rutile (40%) and that of the Al_2O_3 spherules is the α- and γ-phases. Electron-microscopic images of the aggregates were used to measure their equivalent geometrical radius, which is defined as $R = 0.5(LW)^{0.5}$, where L is the maximum length of the aggregate and W is the maximum extent in the direction perpendicular to L. The aggregate morphology was described using the concept of the fractal dimension D_f, which is the exponent in the relation between the aggregate mass M_a and the equivalent geometrical radius R: $M_a \sim R^{Df}$.

Fig. 5 presents the arithmetic mean radius R of aggregates vs. coagulation time, defined as the time elapsed since the specimen combustion was finished up to the sampling moment. Fig. 6 shows an example of the frequency distribution of the Al_2O_3 aggregate radius R after a coagulation time of 1 min. This distribution can be fitted by the lognormal function with standard geometric deviation $\sigma_g = 2.1$.

DOI: 10.13009/EUCASS2019-892

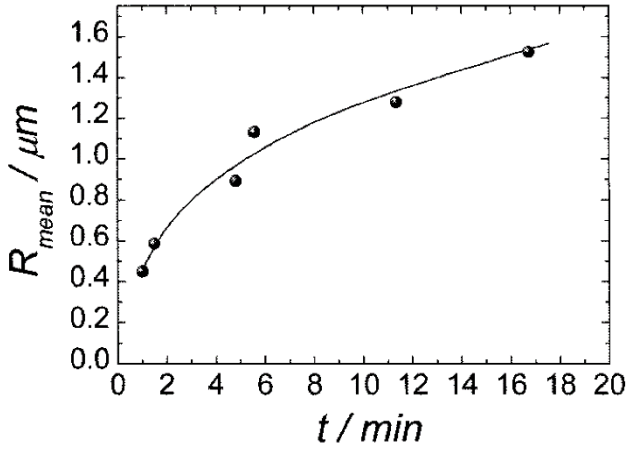

Fig. 5. Arithmetic mean radius of Al_2O_3 aggregates vs. coagulation time (TEM data).

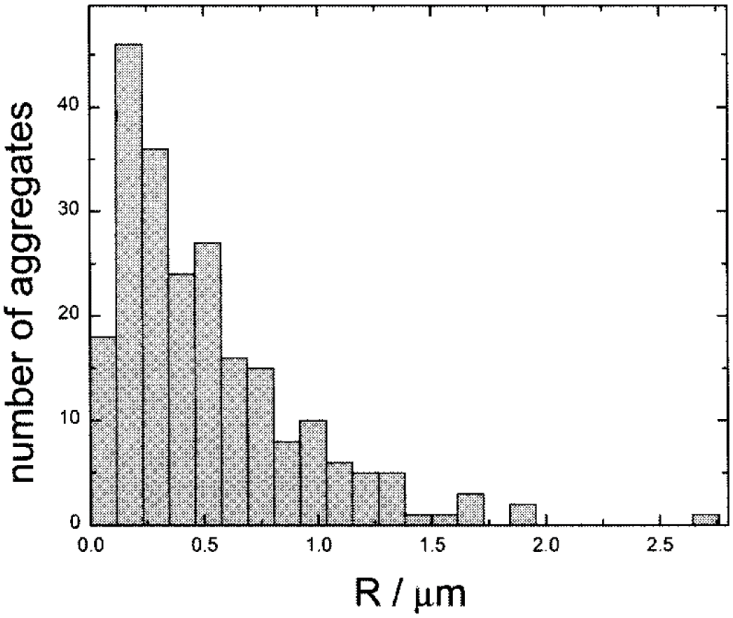

Fig. 6. Frequency distribution of Al_2O_3 aggregate radius R determined from TEM measurements. Coagulation time 1 min. Arithmetic mean radius for this distribution $R_{mean} = 0.45 \pm 0.03$ μm.

The fractal dimension was determined by using two approaches for estimating the aggregate mass. The first approach is based on measuring (in arbitrary units) the integral optical density of a TEM image of the aggregate, which is defined as the sum of the gray values (in the range of 0–255) for all pixels of the aggregate.

It is assumed that the optical density of the image is proportional to the local thickness of the aggregate and the mass is proportional to density. A correction was made for the thickness of the Formvar plate. This method of determining the mass was validated by analytical studies [1], where it was shown that the fractal dimension of a two-dimensional projection of an object is equivalent to the fractal dimension of the three-dimensional object if $D_f < 2$. In the second approach, the diameters of all spherules in the aggregate were measured and the aggregate mass was calculated by multiplying the total volume of the spherules by the density of Al_2O_3/TiO_2. Both approaches give close values of D_f . For TiO_2 aggregates, $D_f = 1.55 \pm 0.1$ (Fig. 7). In the case of Al_2O_3 aggregates, $D_f = 1.6 \pm 0.1$ for particles of size 10, 110, and 340 μm (Fig. 8) and $D_f = 1.8 \pm 0.1$ for particles of size of 4 μm. In addition, it turned out that in both cases (Al_2O_3 and TiO_2), the fractal dimension did not depend on the coagulation time (i.e., the time interval between the sample combustion and sampling) in the examined range of 1–20 min

DOI: 10.13009/EUCASS2019-892

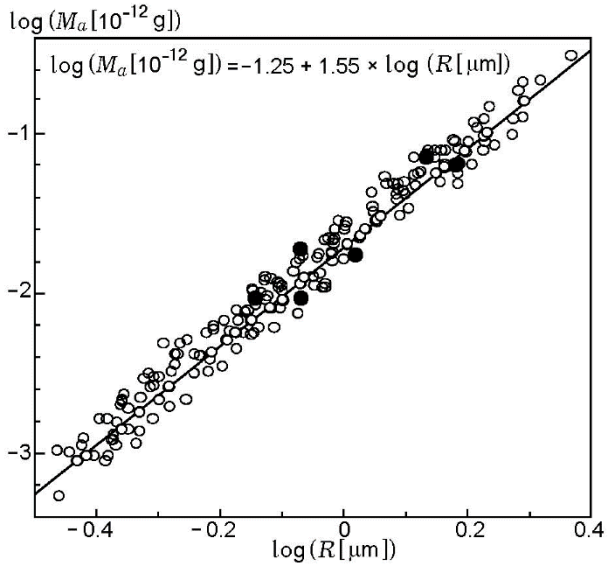

Fig. 7. Mass versus geometrical radius for TiO_2 aggregates: points • indicate that the mass determined by summation of the masses of the primary nanoparticles in the aggregate (from TEM images) and points ◦ indicate that the mass was found by measuring the integral optical density of images of individual aggregates.

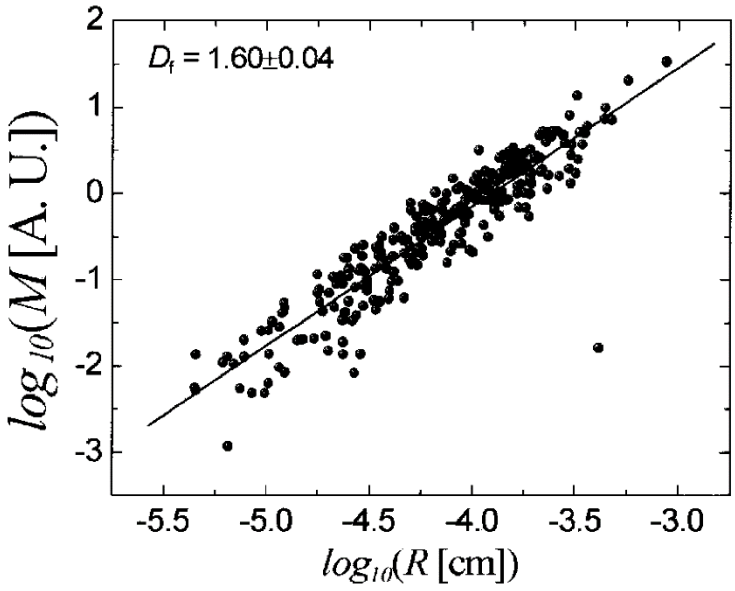

Fig. 8. *M* vs. *R* plots of TEM data for Al_2O_3 aggregates. *M* is the aggregate mass determined by the densitometric elaboration of TEM images; $R = 0.5(LW)^{0.5}$, where *L* and *W* are the dimensions of the rectangle enclosing the images of a single aggregate. The solid line corresponds to the relationship $M \sim R^{Df}$, where $D_f = 1.6$.

In the investigation of the combustion of individual Ti particles, a correlation between the diameter of TiO_2 spherules and the size of the initial Ti particles was not found. Figure 9 gives spherule size distributions for combustion of monodisperse single titanium droplets with a size of 300 μm (experiments of the first type) and titanium particles with sizes less than 20 μm in the pyrotechnic mixture (experiments of the second type). It is evident that the distribution functions are similar and the mean sizes of the primary oxide spherules are close.

In the case of Al particles, it was found that the size distribution of Al_2O_3 spherules is a function of the diameter of the burning metal droplet. Four series of experiments of the first type were conducted with samples generating burning particles with a known size distribution, namely: monodisperse particles with $d_{10} = 340$ μm and $K_{var} = 0.11$, monodisperse particles with $d_{10} = 110$ μm and $K_{var} = 0.14$, polydisperse particles with an

DOI: 10.13009/EUCASS2019-892

effective size 10 μm and K_{var} = 0.54, and particles with a narrow size distribution with d_{10} = 4.0 μm and K_{var} = 0.23. Here $K_{var} = \sigma/d_{10}$ is the coefficient of variation ($\sigma = ((d_{20})^2 - (d_{10})^2)^{0.5}$ is the standard deviation). The size distribution of primary Al_2O_3 particles (Fig. 10) and the dependence of the mean particle radius of primary spherules r_{prim} on the radius $r = d_{10}/2$ of the burning Al particle (Fig. 11) were obtained.

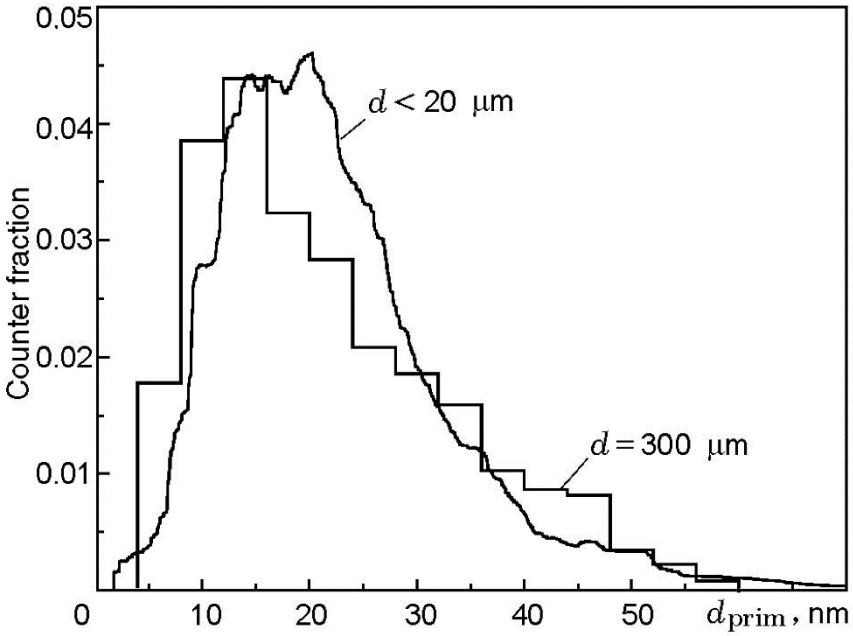

Fig. 9. Size distribution of TiO_2 primary particles in the aggregates produced by combustion of single Ti particles of diameter d = 300 μm (spherule sizes are d_{10} = 22.4 nm and d_{30} = 27.9 nm) and a pyrotechnic mixture with particle sizes d < 20 μm (spherule sizes are d_{10} = 22.7 nm and d_{30} = 28.3 nm).

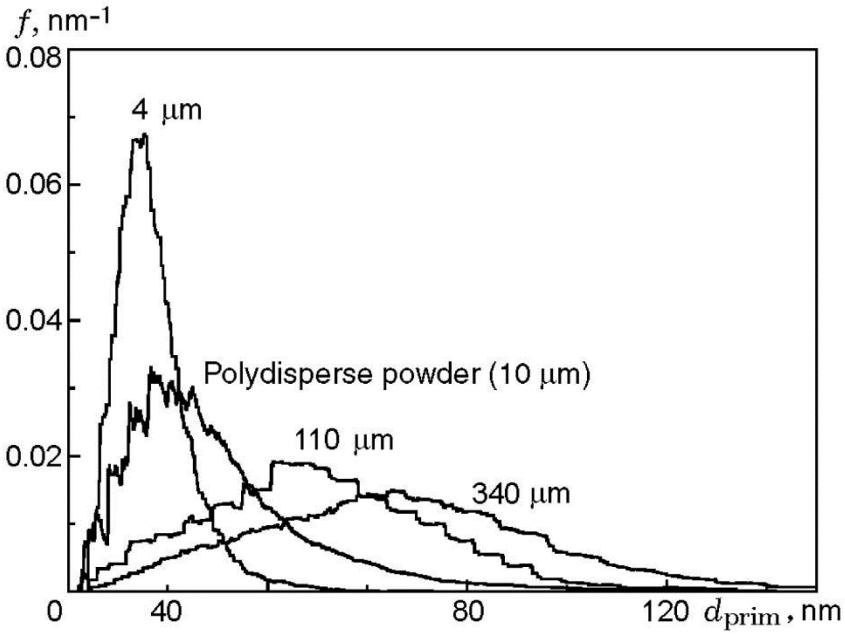

Fig. 10. Size distribution of Al_2O_3 primary particles produced by combustion of pyrotechnic mixtures containing a monodisperse Al powder with particle sizes of 4, 110, and 340 μm and a polydisperse powder with a mean particle diameter of 10 μm.

DOI: 10.13009/EUCASS2019-892

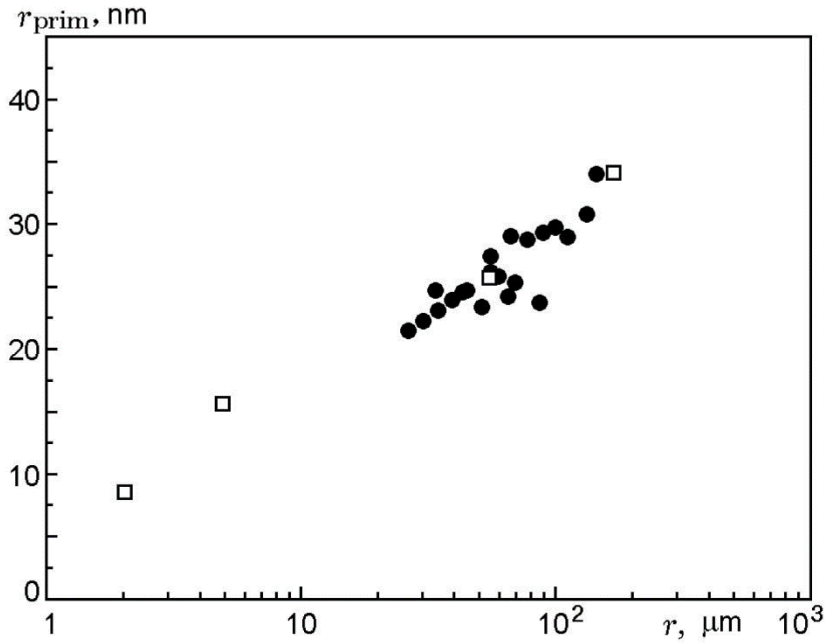

Fig. 11. Mean radius of primary particles versus radius of initial Al particles in the pyrotechnic mixture: points □ refer to experimental data and points • refer to calculations using the analytical model.

Figures 1, 2 show typical images of a burning aluminum droplet. Characteristic features of aluminum particle combustion are the presence of a lens-like oxide cap on the surface and a reaction zone (halo) distant from the surface, where aluminum oxide nanoparticles are formed by the reaction between metal vapor and air oxygen. The radius of the reaction zone R_{reac} (halo) depends on the radius of the burning droplet r (Fig. 12). The burning time of an Al droplet of diameter of about 100 μm in air is 20–30 msec. At the end of combustion, the flame is usually extinguished in 1–3 msec. Approximately 1% of the total number of aluminum particles explode at the end of combustion.

In contrast to Al particles, almost all Ti particles exploded, the series of frames in Fig. 13 illustrates this process. The light segment (track) in the first frame ($\tau = 0$) is the particle trajectory for a time of 0.9 msec. The next frame ($\tau = 1$ msec) shows the moment of particle explosion. It is evident that in $\tau = 1$–3 msec, most of the resulting fragments explode again. In some cases, a series of explosions is observed. Thus, fragment 3, which exploded in the last frame ($\tau = 15$ msec) resulted from the explosion of fragment 2.

We note that, unlike in Al particle combustion, a reaction zone distant from the surface is not observed in combustion of Ti droplet, i.e., the zone of oxide nanoparticle formation is in immediate proximity to the droplet surface.

To obtain data on the early stages of oxide nanoparticle formation, we used "imprints" of the halo and tail zone of the burning metal droplets under their small angle impact on the plate. Figures 14 and 15 show thermophoretic deposits of Al_2O_3 and TiO_2 produced by impact of Al and Ti droplets and the corresponding optical density profiles of these deposits. In the case of aluminum, the density profile has two maxima, which indicates that the reaction zone is at a distance from the particle surface (see also Fig. 1, 2). In the case of titanium droplet combustion, unlike in the case of aluminum, the deposit density declines monotonically with distance from the center. A TEM image of the TiO_2 deposit is shown in Fig. 16. It is evident that single particles and fairly small aggregates are present near the surface and long chain aggregates are observed in the tail zone.

The results demonstrate that there are significant differences between the Ti and Al combustion mechanisms.

DOI: 10.13009/EUCASS2019-892

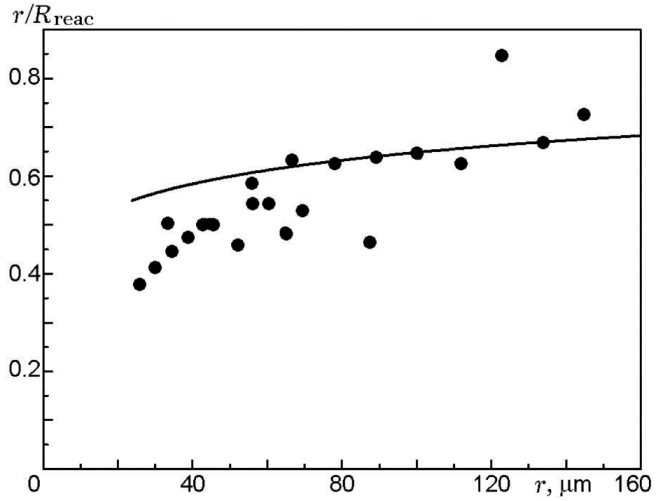

Fig. 12. Ratio of the radius r of a burning Al particle to the halo radius R_{reac} as a function of the Al particle radius (points); the solid curve is an analytical solution.

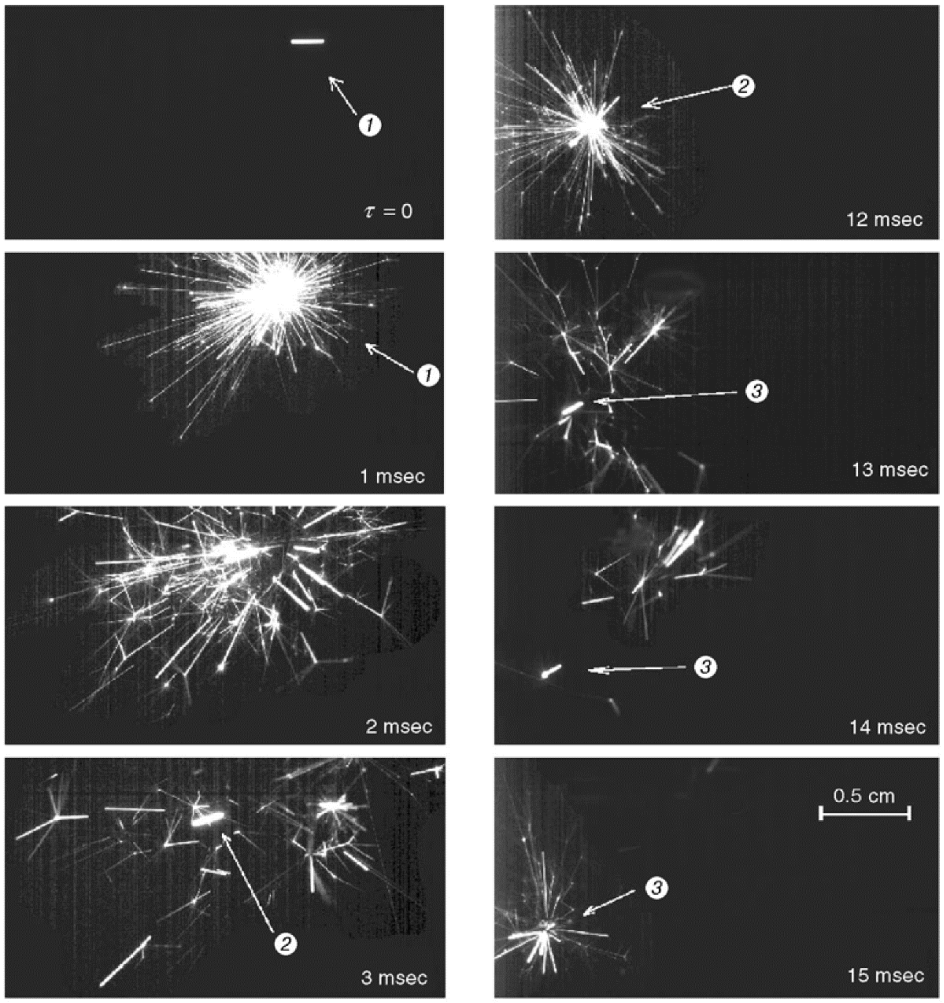

Fig. 13. Sequence of frames illustrating explosion at the end of titanium droplet combustion: the initial diameter of the droplet is 200 μm; the frame exposure time is 0.9 msec; the initial time for each frame is shown in each frame; the exploding fragments are marked by 1–3.

DOI: 10.13009/EUCASS2019-892

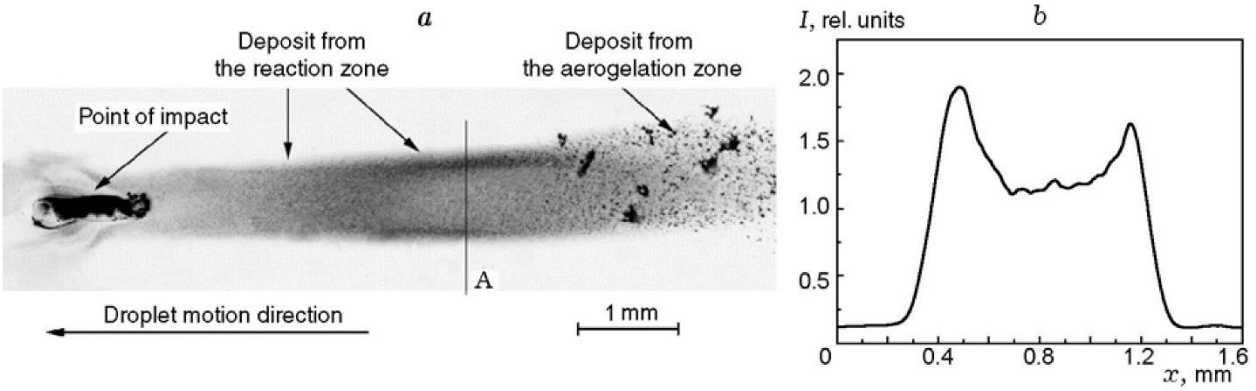

Fig. 14. Deposit from a burning Al particle of initial diameter of 300 μm under small-angle impact of the particle on the plate (a) and the density profile of the Al_2O_3 deposit in section A (b).

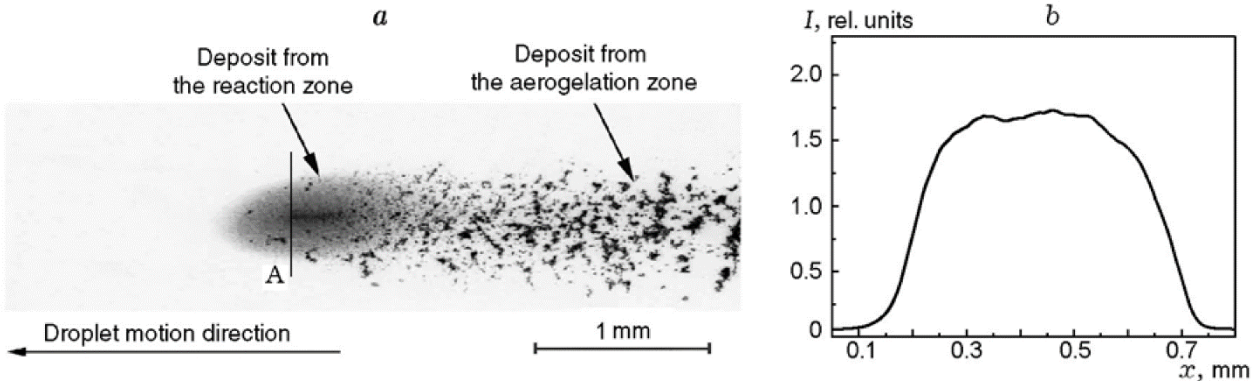

Fig. 15. Deposit from a burning Ti particle of initial diameter 300 μm under small-angle impact of the particle on the plate (a) and the density profile of the TiO_2 deposit from the reaction zone in section A (b).

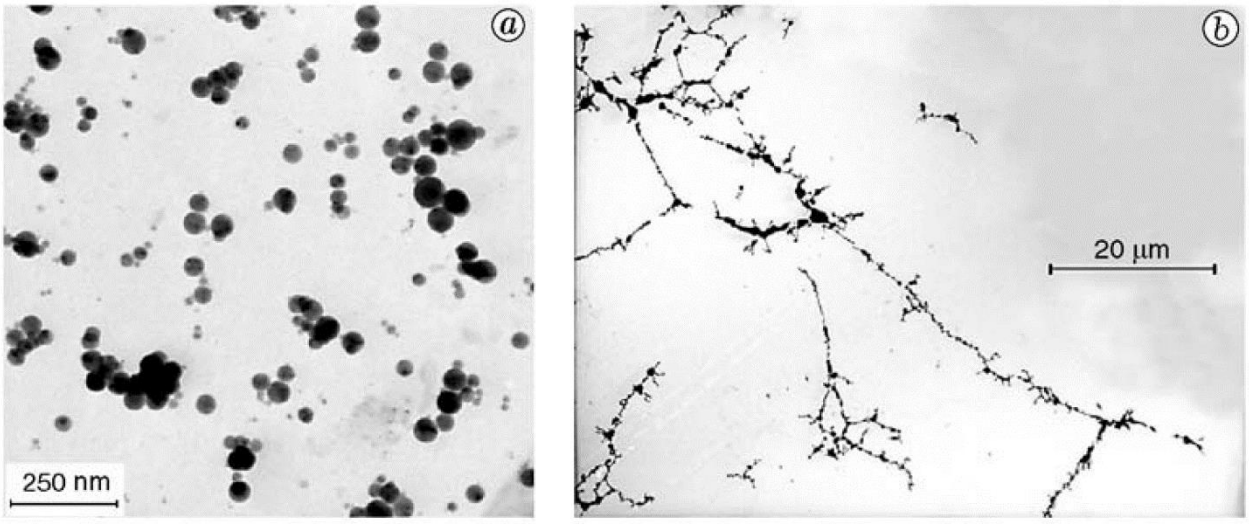

Fig. 16. TEM images of titanium oxide particles from the reaction zone (a) and the aerogelation zone (b).

4. Specific time histories of nanooxide formation during combustion

The main techniques used were: high-speed video registration and local sampling of nano-oxide products. To visualize the oxide smoke “trail” of the burning metal particle, its trajectory was highlighted by several halogen lamps. The local brightness of trail vs coordinate along the trajectory of burning particle was obtained by the longitudinal

DOI: 10.13009/EUCASS2019-892

photometric scanning of the smoke trail image (Fig. 18, 19). It was assumed that the local brightness and the rate of smoke generation have a positive correlation.

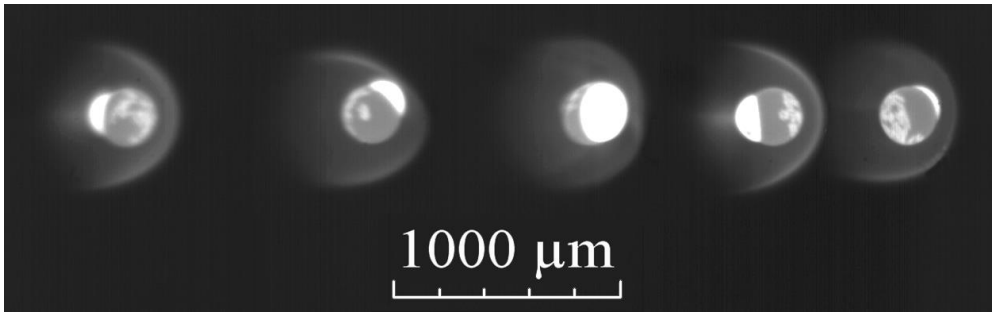

Fig. 17. A set of successive images of a burning 350 micron droplet of aluminum moving in the air, 500 frames per second, rotation is visible.

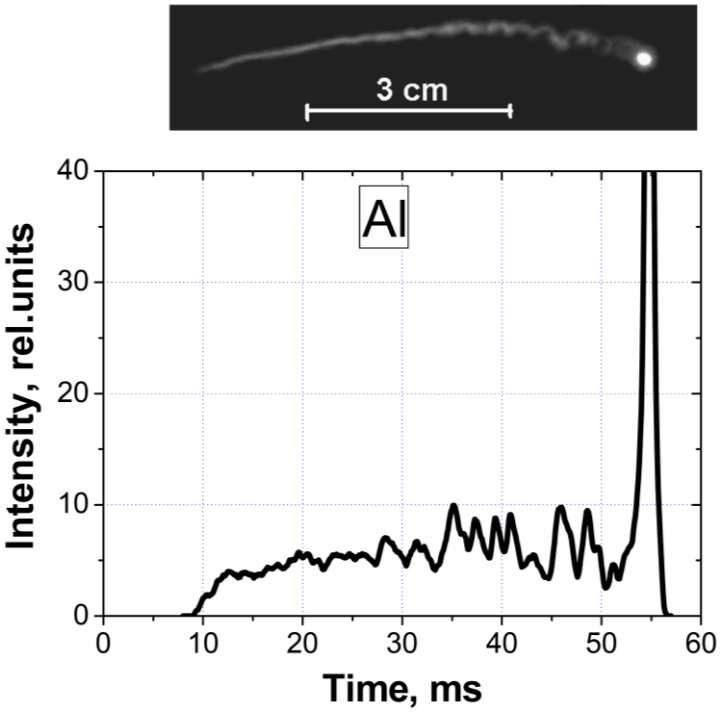

Fig. 18. Burning Al particle with the smoke tail illuminated (top), the photometric scanning of the local brightness of tail along its trajectory (bottom).

DOI: 10.13009/EUCASS2019-892

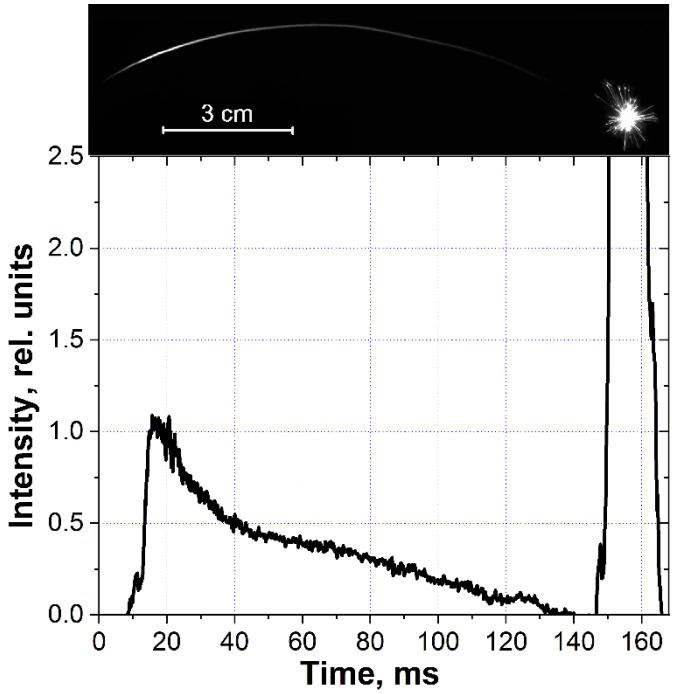

Fig. 19. Burning Ti particle with the smoke tail illuminated (top), the photometric scanning of the local brightness of tail along its trajectory (bottom).

As a result, the smoke formation rate vs. time were obtained during the burning Ti and Al micro particles in air, including the time moments of onset and termination of generation (Fig. 20) and the moment of explosion for Ti particles. A qualitative (semi-quantitative) explanation of the course of these curves is given, taking into account the temperature time traces and the specific burning features for each metal. An explanation for the explosion of a titanium metal particle at the end of combustion is also suggested.

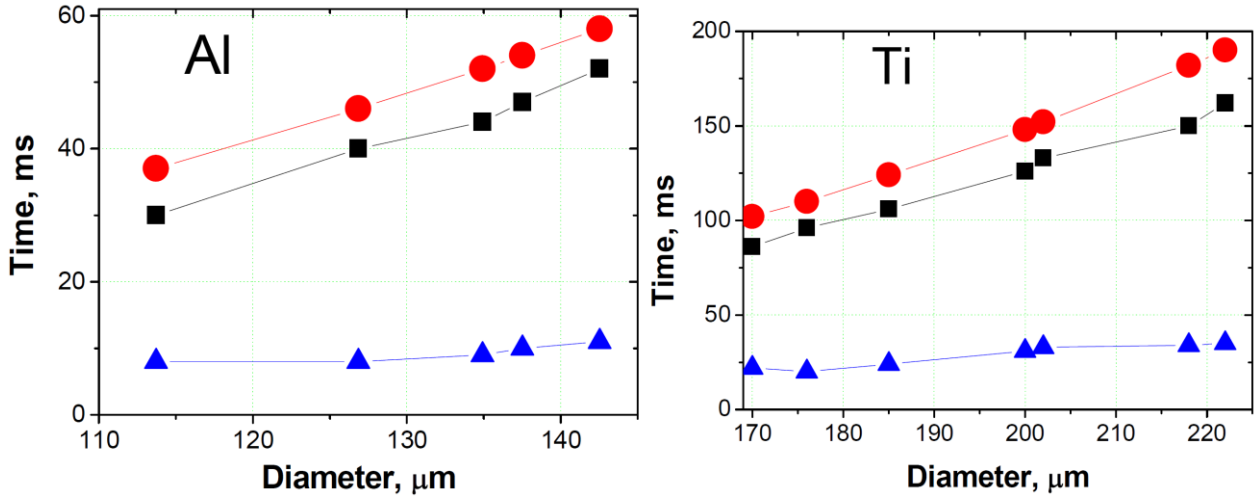

Fig. 20. Time phases of combustion of Al and Ti particles: triangle - the onset of generation of oxide smoke, square - ending of the generation of oxide smoke, circle - total burning time (moment of the extinction or explosion).

5. Rotation of Al particles

It was recorded that the self-luminous streaks of burning Al particles exhibited the periodic brightness oscillations (Fig. 21). As the droplet burns, the frequency of oscillations of the luminous streak increases usually, and also the smoke trail acquires a spiral shape with increasing diameter and frequency of the spiral. In addition, comparing the consecutive frames of the high-speed micro video recording (Fig. 17), it is evident that the drop with a bright oxide

DOI: 10.13009/EUCASS2019-892

cap rotates rapidly enough, that results in the oscillating luminous streak. The registrations of oscillating luminous streaks were also noted in a number of papers on the combustion of Al particles and particles of Al-Mg, Al-B, and Mg-B alloys. [2-5]

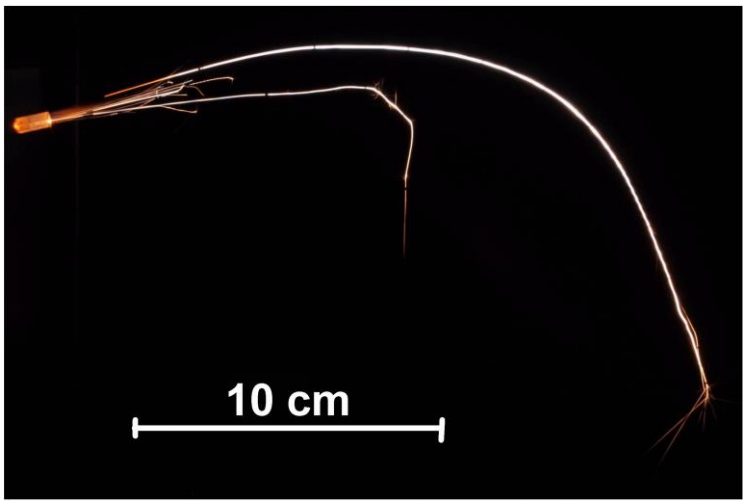

Fig. 21. Photoframe through a chopper disk (for time stamps) of the burning aluminum particles and recording their rotation speed on "undulating" tracks.

The rotation can be explained by the action of an overheated micro-jet of aluminum vapor (or sub oxides) from under the oxide cap, which is directed tangentially to the surface. As a result, it was found that the frequency of rotation is the decreasing function of the Al droplet diameter. The experimental points obtained (for diameters > 100 μm) and points from [4] for Al droplet sizes <100 μm can be well approximated by a unified curve (Fig. 22).

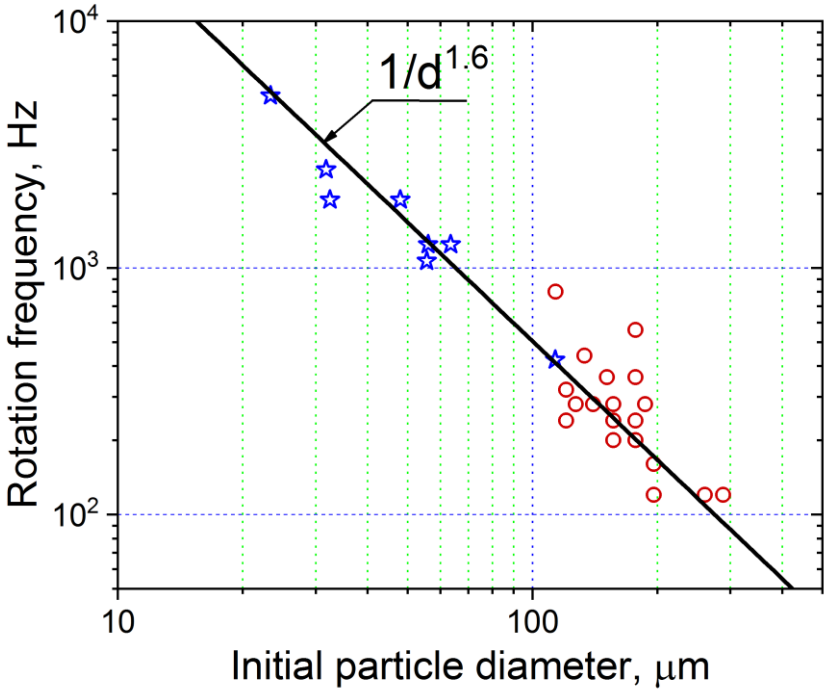

Fig. 22. Frequency of rotation of burning aluminum particles as a function of diameter. Red circles – data obtained in [5], blue stars – data from [4].

Based on the type of rotational motion, a simple model was developed to explain the rotation of the burning Al drop with Al_2O_3 cap (Fig. 23).

DOI: 10.13009/EUCASS2019-892

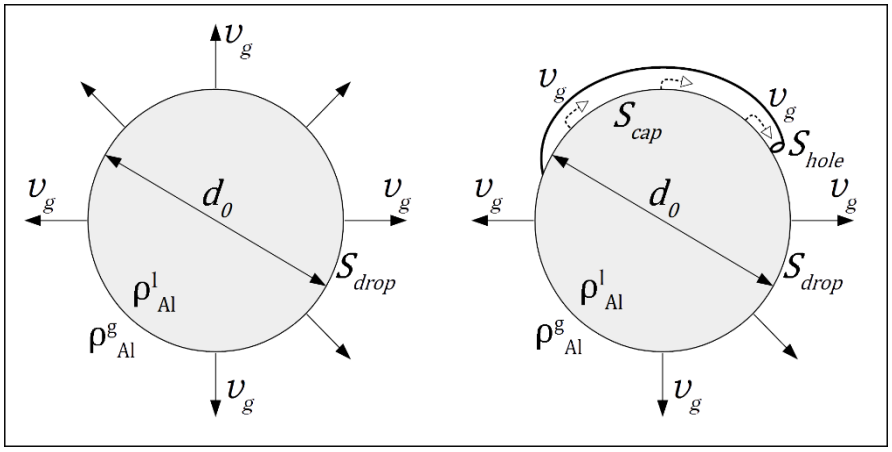

Fig. 23. Scheme explaining the rotation model: left view - Initial moment of combustion, right view – time moment with oxide cap. (Character notations see in the text)

Designation of parameters in the Fig. 23:
v_g – aluminum vapor velocity, ρ^g_{Al}- density of aluminum vapor, ρ^l_{Al}- density of liquid aluminum, d_0 – initial Al particle diameter, S_{drop} – initial Al particle surface area, S_{cap} – area of the Al droplet, covered by oxide cap, S_{hole} – area of the hole, from which the jet of the gas of Al and suboxide ejects.

The law of conservation of mass flux from the surface:

$$v_g S_{drop} t_b \rho^g_{Al} = M_0 = \rho^l_{Al} \frac{\pi d_0^3}{6}$$

The law of combustion [6]:

$$t_b[s] = 7.07 \cdot 10^5 \cdot (d_0[m])^{1.8}$$

Moment of jet force is equal to moment of viscous air resistance [7]:

$$2\pi\mu\omega d_0^3 = \dot{m}_g \frac{S_{cap}}{S_{hole}} v_g d_0,$$

here: μ – air dynamic viscosity, ω – rotation frequency
Mass flow rate of Al suboxides through the hole:

$$\dot{m}_g = \frac{S_{cap}}{S_{drop}} \frac{M_0}{t_b} = \frac{S_{cap}}{S_{drop}} \frac{\pi \rho^l_{Al}}{4.24 \cdot 10^6} (d_0)^{1.2}$$

The dependence of frequency of rotation vs the initial particle diameter:

$$\omega = \frac{S_{cap}^2}{S_{hole} S_{drop}} \frac{\left(\rho^l_{Al}\right)^2}{72 \rho^g_{Al} \mu} \frac{1}{(7.07 \cdot 10^5)^2 d_0^{1.6}} \sim \frac{1}{d_0^{1.6}}$$

Conclusion

The obtained regularities will allow: a) to refine the models of Al, Ti particles combustion to include the kinetics of nano-oxide generation, b) to work out the recommendations on the modification of the combustion mode in order to reduce the size of nanoparticles and to increase the conversion fraction into nano-oxide.

Acknowledgements

The work was supported by the Russian Foundation for Basic Research (project № 19-03-00294).

References

[1] Friedlander, S. K. (2000). Smoke Powder and Haze.
[2] Wang, S., Schoenitz, M., & Dreizin, E. L. (2017). Combustion of boron and boron-containing reactive composites in laminar and turbulent air flows. Combustion Science and Technology, 189(4), 683-697.
[3] Aly, Y., Schoenitz, M., & Dreizin, E. L. (2013). Ignition and combustion of mechanically alloyed Al–Mg powders with customized particle sizes. Combustion and Flame, 160(4), 835-842.

DOI: 10.13009/EUCASS2019-892

[4] Zepper, E. T., Pantoya, M. L., Bhattacharya, S., Marston, J. O., Neuber, A. A., & Heaps, R. J. (2017). Peering through the flames: imaging techniques for reacting aluminum powders. Applied optics, 56(9), 2535-2541.
[5] Karasev V. V., Valiulin S. V., Reshetnikov I. V., Bykovskikh A. M., Kalinina A. E. (2018). Specific time histories of nanooxide formation during combustion of Al and Ti microparticles, Energetic Materials Synthesis, Processing, Performance: 49rd International Annual Conference of Fraunhofer ICT, P 130.
[6] Beckstead, M. W., Liang, Y., & Pudduppakkam, K. V. (2005). Numerical simulation of single aluminum particle combustion. Combustion, Explosion and Shock Waves, 41(6), 622-638.
[7] Fuks, N. A. (1989). The mechanics of aerosols. Dover Publications.